CMB constraints on a stochastic background of primordial magnetic fields

Daniela Paoletti and Fabio Finelli

Phys. Rev. D **83**, 123533 — Published 29 June 2011

DOI: 10.1103/PhysRevD.83.123533

CMB Constraints on a Stochastic Background of Primordial Magnetic Fields

Daniela Paoletti*
Dipartimento di Fisica and INFN,
università degli Studi di Ferrara,
via Saragat, 2 I-44100 Ferrara - Italy and
INAF/IASF-BO,Istituto di Astrofisica Spaziale e Fisica Cosmica di Bologna
via Gobetti 101, I-40129 Bologna - Italy

Fabio Finelli†
INAF/IASF-BO, Istituto di Astrofisica Spaziale e Fisica Cosmica di Bologna
via Gobetti 101, I-40129 Bologna - Italy and
INFN, Sezione di Bologna, Via Irnerio 46, I-40126 Bologna, Italy

We constrain a stochastic background of primordial magnetic field (PMF) by its contribution to the angular power spectrum of cosmic microwave background anisotropies. We parametrize such stochastic background by a power-law spectrum with index n_B and by its Gaussian smoothed amplitude B_λ on a comoving length λ. We give an approximation for the spectra of the relevant correlators of the energy-momentum of the stochastic background of PMF for any n_B. By using the WMAP 7 year data in combination with ACBAR, BICEP and QUAD we obtain the constraint $B_{1\rm Mpc} < 5.0$ nG at 95% confidence level for a stochastic background of non-helical PMF. We discuss the relative importance of the scalar and vector contribution to CMB anisotropies in obtaining these constraints. We then forecast PLANCK capabilities in constraining $B_{1\rm Mpc}$.

I. INTRODUCTION

The origin of the large scale magnetic fields observed in galaxies and clusters of galaxies is an open issue of great importance in modern astrophysics (see [1] for a review). Primordial magnetic fields (PMF) generated in the early Universe could have been the seeds for large scale magnetic fields and have left an imprint in the anisotropy pattern of the cosmic microwave background (CMB). A primordial hypothesis for generating the seeds amplified afterwards by adiabatic compression and dynamo - cannot be discarded [1], also in light of recent observations of strong magnetic fields in galaxies at high redshift [2, 3].

PMF with a comoving amplitude of several nG can leave interesting imprints on CMB anisotropies. A stochastic background of PMF is modelled as a fully inhomogeneous component and its energy momentum tensor (EMT) - quadratic in the magnetic fields - is considered at the same footing as linear inhomogeneities in the other components and linear metric fluctuations. A stochastic background of PMF generates independent modes for all kinds of linear perturbations: there has been several studies for scalar [4–11], vector [12–14] and tensor [13, 15, 16] perturbations. See Refs. [9, 10] for studies which take into account all the types of contributions. A stochastic background of PMF affects also the statistics of CMB anisotropies, and not only its power spectra: being quadratic in the magnetic field amplitude, the EMT is non-Gaussian distributed [17] and therefore the bispectrum of CMB anisotropies can also be a useful probe [18, 19].

In our previous works [8, 9] we have refined the computation of CMB anisotropies in presence of a stochastic background of PMF: we have computed the initial conditions for cosmological perturbations in the radiation era keeping into account only relativistic degrees of freedom and the correlators for the Fourier transforms of the EMT in presence of a sharp cut-off which mimics the damping scale due to viscosity [8, 9] for few values of the spectral index n_B of the stochastic background.

In this paper we use and extend the above theoretical description to derive the CMB constraints on a stochastic background of PMF which can be obtained by current and future data. We therefore use a modified version of `CosmoMC` [20] connected with a modified version of `CAMB` [21] containing all the above features to constrain B_λ - the amplitude of the magnetic field smoothed over a comoving scale λ - and n_B with the most recent compilation of CMB anisotropies data, therefore updating previous investigations [5, 22, 23]. We also forecast the PLANCK [24] capabilities in constraining such a background of PMF.

Our paper is organized as follows. In Section II we present the theoretical set-up needed for deriving the CMB constraints. As new results we give an approximation for the PMF energy-momentum valid for any n_B, we discuss the correlator between the energy density and the Lorentz force and we extend the regular initial conditions for cosmological perturbations in the relativistic regime in presence of a stochastic background of PMF [9] including the correction due to matter, collecting the details in Appendix A, B and C, respectively. In Section III we discuss the constraints from WMAP 7 years data [25, 26], ACBAR [27], BICEP [28] and QUAD [29] on a flat ΛCDM model plus a stochastic background of PMF. We present the Planck capabilities in constraining B_λ and n_B in Section IV and we summarize our results

* paoletti@iasfbo.inaf.it
† finelli@iasfbo.inaf.it

in Section V.

II. STOCHASTIC BACKGROUND OF PMF

A stochastic background of PMF acts as a fully inhomogeneous source to the Einstein equations. As usual, we assume the infinite conductivity limit in which the PMF simply scales with time as $B(\mathbf{x},\tau) = B(\mathbf{x})/a(\tau)^2$ where $a(\tau)$ is the scale factor normalized to $a_0 = 1$ today and τ is the conformal time. We model PMF with a power-law spectrum $P_B(k) = A\,k^{n_B}$. The two point correlation function for inhomogeneous fields is:

$$\langle B_i(\mathbf{k}) B_j^*(\mathbf{k}')\rangle = (2\pi)^3\delta(\mathbf{k}-\mathbf{k}')(\delta_{ij}-\hat{k}_i\hat{k}_j)\frac{P_B(k)}{2} \quad (1)$$

where $n_B > -3$ to avoid infrared singularities. Magnetic perturbations survive the Silk damping but on smaller scales PMF are damped by radiation viscosity. We model this damping introducing a sharp cut off in the spectrum at a damping scale k_D [12] which is much smaller than the Silk scale. To parametrize PMF amplitude, we choose to use the most common convention which smooths the magnetic fields with a Gaussian filter over a comoving scale λ:

$$B_\lambda^2 = \int_0^\infty \frac{dk\,k^2}{2\pi^2} e^{-k^2\lambda^2} P_B(k) = \frac{A}{4\pi^2\lambda^{n_B+3}}\Gamma\left(\frac{n_B+3}{2}\right) \quad (2)$$

As damping scale we adopt the proposal of Ref. [12], in which k_D is function of B_λ and the spectral index n_B:

$$k_D = (2.9\times10^4)^{\frac{1}{n_B+5}}\left(\frac{B_\lambda}{\mathrm{nG}}\right)^{\frac{-2}{n_B+5}}\left(\frac{2\pi}{\lambda/\mathrm{Mpc}}\right)^{\frac{n_B+3}{n_B+5}} h^{\frac{1}{n_B+5}}\,. \quad (3)$$

The EMT of PMF is a source term for the Einstein-Boltzmann system and, being these quadratic in the $B_i(\mathbf{k})$, the Fourier transfoms of the EMT components are convolutions [13, 15]:

$$|\rho_B(k)|^2 = \frac{1}{1024\pi^5}\int_\Omega d\mathbf{p} P_B(p)\,P_B(|\mathbf{k}-\mathbf{p}|)(1+\mu^2)^2 \quad (4)$$

$$|\Pi^{(V)}(k)|^2 = \frac{1}{512\pi^5}\int_\Omega d\mathbf{p} P_B(p)\,P_B(|\mathbf{k}-\mathbf{p}|) \times[(1+\beta^2)(1-\gamma^2)+\gamma\beta(\mu-\gamma\beta)] \quad (5)$$

$$|\Pi^{(T)}(k)|^2 = \frac{1}{512\pi^5}\int_\Omega d\mathbf{p} P_B(p) P_B(|\mathbf{k}-\mathbf{p}|) \times(1+2\gamma^2+\gamma^2\beta^2)\,, \quad (6)$$

where $\mu = \hat{\mathbf{p}}\cdot(\mathbf{k}-\mathbf{p})/|\mathbf{k}-\mathbf{p}|$, $\gamma = \hat{\mathbf{k}}\cdot\hat{\mathbf{p}}$, $\beta = \hat{\mathbf{k}}\cdot(\mathbf{k}-\mathbf{p})/|\mathbf{k}-\mathbf{p}|$ and Ω denotes the volume with $p < k_D$.

The analytical exact results for Eqs. (4-6) are given for specific values of n_B in our previous papers [8, 9]. However, the expressions for generic n_B are rather complicated and cannot be used in a numerical implementation. Therefore we fitted the analytical results with easier expressions to be inserted as spectra for the PMF in modified version of `CAMB` [21] and `CosmoMC` [20]. Since the spectral shape varies with the spectral index we had to divide the spectra in different index ranges. The first natural split is between indices greater and smaller than $n_B = -3/2$: this division is very natural since is required by the change in the infrared behaviour between the two ranges. In order to achieve the best accuracy with the fits and considered the wide range of spectral indices that we wanted to explore we decided to do a further splitting in the $n_B > -3/2$ range between positive and negative spectral indices. In the end we result into three different spectral fits for each EMT component. In Fig.1 we show respectively for scalar energy density, scalar Lorentz force and vector anisotropic stress the results of our fits compared with the analytical results. We note how the fits are in excellent agreement with the analytical results and we refer the reader to Appendix A for the details. In the next two subsections we address other two issues related to the theoretical characterization of a stochastic background of PMF, recently addressed in Refs. [10, 30].

A. Cross-Correlation between Lorentz Force and Energy Density

The first issue is represented by the cross correlation between Lorentz force and magnetic energy density as pointed out in [10]. In particular the analysis of the magnetized scalar mode involves three quantities: magnetic energy density, Lorentz force and anisotropic stress. These quantities are not independent one from the other but are related throught the conservation equation for the PMF EMT (in the magnetic hydrodynamic limit): $\sigma_B = \frac{\rho_B}{3} + L_B$. We approximated the Lorentz force and the magnetic energy density as anti-correlated [8, 9], however, the Lorentz force and the magnetic energy density correlation can be calculated, as for the their auto-correlations, as pointed out in Ref. [10]. The cross-correlator between ρ_B and L_B is given by:

$$\langle\rho_B(\mathbf{k})L_B(\mathbf{k}')\rangle = \frac{\delta(\mathbf{k}-\mathbf{k}')}{1024\pi^5}\int d\mathbf{p} P_B(p)\,P_B(|\mathbf{k}-\mathbf{p}|) \times(1-1(\gamma^2+\beta^2)+2\gamma\beta\mu-\mu^2)^2 \quad (7)$$

The above formula can be computed analitycally and in the appendix we show the analytical results both for $n_B = -2.5$ and $n_B = 2$. The general behavior in the large scale limit of the spectrum (for $k << k_D$), the range relevant for CMB anisotropies, is:

$$\langle\rho_B(k)L_B(k)\rangle = -\frac{1}{3}|\rho_B(k)|^2 \text{ for } n_B \geq -3/2$$
$$\langle\rho_B(k)L_B(k)\rangle = -C|\rho_B(k)|^2 \text{ for } n_B < -3/2$$

where $C \sim \mathcal{O}(1)$. In the appendix we show that the exact evaluation of the cross correlation has a small effect - in particular for strongly negative n_B - with respect to our choice of considering the Lorentz force and the energy density as fully anti-correlated.

B. Magnetized Scalar Initial Conditions with matter Corrections

The second issue is related with the initial conditions for magnetized scalar perturbations. In our previous works [8, 9] we computed the intial conditions in the approximation of a universe dominated by radiation, following the results presented in Ref. [30] we investigated the importance of matter contributions to initial conditions. We computed the initial conditions with the inclusion of matter corrections and we give the details in appendix C. The results show that the introduction of matter corrections in the initial conditions have a negligible impact on the numerical computation of the magnetized scalar CMB anisotropies.

III. CONSTRAINTS FROM CURRENT CMB DATA

We derived the constraints on PMF with current CMB anisotropy data performing an analysis of the WMAP 7 year [25, 26], ACBAR [27] data in temperature and of the BICEP [28] and QUaD [29] data in polarization. In order to decrease the correlations between different data sets which cover the same region of the sky, we proceed as in Ref. [31]. We remove in the analysis the following CMB band powers: a) all the QUaD TT band powers since they overlap with data from the 'CMB8' region of ACBAR, b) the ACBAR band powers with $\ell < 910$ and $\ell > 1950$ to avoid overlap with WMAP (which is cosmic variance limited up to $\ell = 919$ [25, 26]) and contamination from foreground residuals,respectively, c) the QUAD TE band powers which overlap with WMAP ones, the QUAD EE band powers which overlap with BICEP, d) the BICEP TT, TE band powers (i.e., we use just EE and BB information from BICEP).

We use a modified version of `CosmoMC` [20] in order to compute the Bayesian probability distribution of cosmological parameters, including the magnetic ones. We vary the baryon density $\omega_b = \Omega_b h^2$, the cold dark matter density $\omega_c = \Omega_c h^2$ (with h being $H_0/100\mathrm{km\,s^{-1}Mpc^{-1}}$), the reionisation optical depth τ (not to be confused with the conformal time τ), the ratio of the sound horizon to the angular diameter distance at decoupling θ, $\ln(10^{10}A_S)$, n_S and the magnetic parameters $B_{|1\mathrm{Mpc}}$ (in units of 10nG) and n_B. As priors we use $[0\,,10]$ for $B_{1\mathrm{Mpc}}/(10\mathrm{nG})$ and $[-2.9\,,3]$ for n_B. The damping scale k_D defined in Eq. (3) is obtained as a derived parameter (in units of Mpc^{-1}), as well as H_0.

We assume a flat universe, a CMB temperature $T_{\mathrm{CMB}} = 2.725$ K and we set the primordial Helium fraction to $y_{\mathrm{He}} = 0.24$. We use the recombination routine RECFAST v1.5 [32]. We restrict our analysis to three massless neutrinos (a non-vanishing neutrino mass leads to a large scale enhancement in the power spectrum of CMB anisotropies in the presence of PMF [10] and would not change our results). The pivot scale of the primordial scalar was set to $k_* = 0.05$ Mpc^{-1}. In order to fit WMAP 7 years, ACBAR and QUaD data, we use the CMB power spectra and we follow the method implemented in `CosmoMC` consisting in varying a nuisance parameter A_{SZ} which accounts for the unknown amplitude of the thermal Sunyaev-Zeldovich (SZ) contribution to the small-scale CMB data points assuming the model of [37]. We use a `CAMB` accuracy setting of 1. We sample the posterior using the Metropolis-Hastings algorithm [38] at a temperature $T = 2$ (the temperature parameter in the `CosmoMC` code is used to sample the probability P as $P^{1/T}$, allowing a better exploration of the distribution tails), generating four parallel chains and imposing a conservative Gelman-Rubin convergence criterion [39] of $R - 1 < 0.01$.

In Table I are reported the results of our analysis on current CMB data. We compare the results for the six standard cosmological parameters both considering or not the PMF contribution. The comparison shows that

Parameter	Mean $B_\lambda = 0$	Mean
ω_{b}	$0.0222^{+0.0011}_{-0.0010}$	0.0222 ± 0.0010
ω_{c}	$0.109^{+0.010}_{-0.009}$	0.109 ± 0.010
θ	$1.040^{+0.004}_{-0.005}$	$1.040^{+0.004}_{-0.005}$
τ_{dec}	$0.086^{+0.030}_{-0.027}$	$0.086^{+0.029}_{-0.030}$
$\log\left[10^{10}A_{\mathrm{S}}\right]$	$3.06^{+0.06}_{-0.07}$	$3.05^{+0.07}_{-0.06}$
n_{S}	$0.956^{+0.024}_{-0.025}$	$0.956^{+0.025}_{-0.026}$
$B_{1\mathrm{Mpc}}/\mathrm{nG}$	...	< 5.0
n_{B}	...	< -0.12
$H_0/\mathrm{km\,s^{-1}Mpc^{-1}}$	$71.5^{+4.6}_{-4.3}$	$74.4^{+4.6}_{-5.4}$

TABLE I. Mean parameter values and bounds of the central 95%-credible intervals without (left column) and with (right column) PMF. Note that H_0 is a derived parameter.

Instrument	LFI	HFI	
Center frequency GHz	70	100	143
Mean FWHM (arcmin)	13.0	9.6	7.0
$\Delta T/T$ per FWHM^2 (Stokes I)	4.45	2.12	1.56
$\Delta T/T$ per FWHM^2 (Stokes $Q\&U$)	6.29	3.39	2.90

TABLE II. Planck channels considered in this analysis and relative performances in the extended mission (four surveys).

Parameter	Input value	Mean
ω_{b}	0.0227	0.0227 ± 0.0003
ω_{c}	0.108	$0.108^{+0.003}_{-0.002}$
θ	...	1.040 ± 0.001
τ_{dec}	0.089	$0.089^{+0.010}_{-0.008}$
$\log\left[10^{10}A_{\mathrm{S}}\right]$	3.1	$3.08^{+0.02}_{-0.01}$
n_{S}	0.960	0.961 ± 0.008
$B_{1\mathrm{Mpc}}/\mathrm{nG}$	...	< 2.7
n_{B}	...	< -0.05
$H_0/\mathrm{km\,s^{-1}Mpc^{-1}}$	72.4	72.3 ± 1.3

TABLE III. Input and mean parameter values with bounds of the central 95%-credible intervals for the Planck simulated data. Note that H_0 is a derived parameter.

neither the means nor the bounds of the cosmological parameters of the ΛCDM model with reionization are basically affected by the presence of PMF: this means that B_λ and n_B are not degenerate with the other six parameter of the concordance cosmological model.

In Figs. 4 and 5 we show the plots of the MCMC results. We derive the following constraints on the amplitude and spectral index of PMF: $B_{1\rm Mpc} < 5.0$ nG and $n < -0.12$ at 95% confidence level.

In Fig. 5 we compare the results obtained including or excluding the scalar contribution. We note how, as expected from previous results on CMB anisotropies [5, 8, 9], the scalar contribution has a very little impact on the constraints on the amplitude B_λ and spectral index n_B. This is due to the different shape of the CMB temperature spectra induced by the scalar and vector contribution of a stochastic background of PMF: compared to the CMB anisotropies sourced by the adiabatic mode, the PMF scalar mode is the dominant contribution on large scales, whereas the vector is the important one at high multipoles. Since the PMF contribution does not suffer of the Silk damping, only the vector contribution has the main chance to affect the CMB temperature sourced by the standard adiabatic mode.

A stochastic background of PMF has also an impact on the matter power spectrum as shown in [8, 10]. In order to investigate if the addition of matter power power spectrum data could improve the constraints on the PMF, we perfomed a MCMC analysis adding the large scale structure (LSS) data of SDSS LRG DR4 [34] to the CMB anisotropy data used before. We used the DR4 release because the DR7 requires the use of non-linear tools to compute the matter power spectrum which are unavailable for ΛCDM plus PMF. We have verified that the addition of the SDSS data does not introduce any significant improvement on the constraints on PMF amplitude. The reason for the lack of improvement is that the matter power spectrum data reach scales of the order of $0.2\,h{\rm Mpc}^{-1}$ where only PMF with positive spectral index have an impact, but PMF with blue spectral indices are already strongly constrained with CMB anisotropy data, therefore the results do not show any significant improvement. This result of a negligible impact of SDSS DR4 data with respect to current CMB data is in agreement with [23].

Let us compare our constraints with other investigations. After our manuscript appeared on the archive, Shaw and Lewis obtained similar CMB constraints - of the order of 6 nG at 95% confidence level - with similar data sets in Ref. [23]. In [22] stronger constraints of the order of 3 nG at 95% confidence level were reported. The reason for slightly different result might be either in the different datasets or in the different methodology used. Concerning the use of matter power spectrum, the present manuscript and Ref. [23] agree that LSS data add very little to CMB current constraints, when only linear scales are correctly included: we obtain analogous results either with SDSS DR4 [34] or 2dF [35], without changing the CMB constraints in Table I. Another difference might be in the use of CBI data [33] in [22], whose foreground contamination at high ℓ has been stressed in Ref. [27]: we believe that the difference might be due to either methodology and/or to the different use of CMB data.

Let us end this section by commenting on the constraints on the magnetic spectral index we derive, i.e. $n_B < -0.12$ at 95% confidence level. This would imply that positive values for n_B are disfavoured and so would be causal mechanism which would have produced such PMF [42]. Certainly there is a trend in $B_\lambda\,, n_B$ which allows for larger B_λ for negative values of n_B: if we fix n_B to the causal value of 2 we obtain a much stronger constraint on the amplitude, i.e. $B_{1\rm Mpc} < 0.023$ nG 95% confidence level. At the same time, we have verified that for undectatable values by CMB of $B_{1\rm Mpc}$ - fixed to 10^{-6} nG - no constraints are derived for n_B, as expected. The above results are obtained by the assumption of a linear prior on $B_{1\rm Mpc}$. We have also performed just for comparison cosmological parameter extraction by sampling ${\rm Log}_{10}[B_{1\rm Mpc}/(10{\rm nG})]$ in the range $[-7, 1]$ [43] and we show the posteriors in Fig. 6. Since the log prior overweights the importance of small amplitudes for $B_{1\rm Mpc}$ compared to the linear prior, the constraints obtained on $B_{1\rm Mpc}$ by sampling logarithmically are tigher - 1 nG at 95% confidence level - , but depend strongly on the interval. As byproduct of the importance given to small amplitude for $B_{1\rm Mpc}$ in sampling logarithmically, n_B is unconstrained. Similar prior issues occur for other important cosmological parameters which are under the threshold of detection, as the amplitude of gravitational waves in standard inflationary scenarios [44].

IV. FORECASTS FOR PLANCK

In the perspective of the forthcoming Planck [24] data we performed a MCMC analysis using simulated Planck data. We created the mock data considering the updated angular resolution and sensitivities [40, 41] for the extended and approved mission duration of four sky surveys, which are summarized in Table II. We used the combination of the three central frequency channels where the CMB is dominant with respect to foreground contributions: 70 GHz, 100 GHz, 143 GHz, which have been combined with the inverse noise variance weighting technique. We used the 92 % of the sky and assumed only CMB neglecting all possible foreground contamination. In Table III we report the results for cosmological parameters with the input parameters of the fiducial model which we choose very close to the WMAP 7 yrs best fit model without PMF.

In Fig. 7 we show the comparison between the parameters constrained by current CMB data and the ones which will be constrained by Planck: note the great improvement given by Planck on the constraints on cos-

mological parameters in presence of PMF. We forecast the following constraints by PLANCK: $B_{1\mathrm{Mpc}} < 2.7$ nG and $n_B < -0.054$ at 95% confidence level. The improvement obtained by PLANCK alone on the constraint on B_λ is mainly due to the better measurement of the CMB temperature anisotropies at high multipoles. The factor of 2 improvement in the constraints on B_λ reached by PLANCK corresponds to a factor 16 improvement in the characterization of C_ℓ.

V. CONCLUSIONS

We studied the constraints on a stochastic background of PMF by current and forthcoming CMB data. In doing this, we have improved the theoretical CMB predictions in presence of a stochastic background of PMF. We gave approximations for the relevant components of the EMT for any spectral index n_B. We considered the correlation between ρ_B and L_B and showed how the previous choice of total anti-correlation [8, 9] was a rather good approximation, in particular for red values of n_B. We computed the initial conditions for magnetic scalar mode in presence of matter corrections showing how these corrections do not affect the results contrary to what claimed in [30].

On the basis of previous works, we have considered only the scalar and vector contribution, and by using their regular initial condition, we constrain $B_{1\mathrm{Mpc}} < 5.0$ nG and $n_B < -0.12$ at 95% confidence level. with the most updated combination of CMB anisotropies. PLANCK will be able to constrain the spectrum of a stochastic background of PMF even further at the level of 2.7 nG.

Acknowledgments

We wish to thank C. Caprini, R. Durrer, J. Hamann and L. Hollenstein for useful comments. This work has been done in the framework of the PLANCK LFI activities and is partially supported by ASI contract PLANCK LFI activity of Phase E2. We acknowledge the use of the Legacy Archive for Microwave Background Data Analysis (LAMBDA). Support for LAMBDA is provided by the NASA Office of Space Science.

Appendix A: PMF EMT spectral fits

Since the spectral behaviour is rather complicated, in order to have the best fit possible we decided to divide the fits for spectral index ranges. Together with the natural separation between indices smaller and greater than $-3/2$, which is necessary due to the completely different behaviour, we added a further separation between negative and positive spectral indices. The leading terms remain the same as in the infrared limit of the exact spectra: white noise for blue indices and infrared dominated for the red ones.

1. Scalar Spectra

$n_B \geq 0$

$$|\rho_B(k,n_B)|^2_{fit} = \frac{A^2 k_D^{2n_B+3}}{512\pi^4 k_*^{2n_B}}\Big(\frac{4}{2n_B+3} - \tilde{k} + \sum_{i=1}^{3} A_i \tilde{k}^{i+1} + A_4 \tilde{k}^{(2n_B+3)}\Big) \tag{A1}$$

$-3/2 < n_B < 0$

$$|\rho_B(k,n_B)|^2_{fit} = \frac{A^2 k_D^{2n_B+3}}{512\pi^4 k_*^{2n_B}}\Big(\frac{4}{2n_B+3} - \tilde{k} + \sum_{i=1}^{3} B_i \tilde{k}^{i+1} + B_4 \tilde{k}^{(2n_B+3)}\Big) \tag{A2}$$

$-2.9 < n_B < -3/2$

$$|\rho_B(k,n_B)|^2_{fit} = \frac{A^2 k_D^{2n+3}}{512\pi^4 k_*^{2n_B}}\Big(\frac{4}{2n_B+3} - \tilde{k} + C_1 \tilde{k}^{(2n_B+3)}\Big) \tag{A3}$$

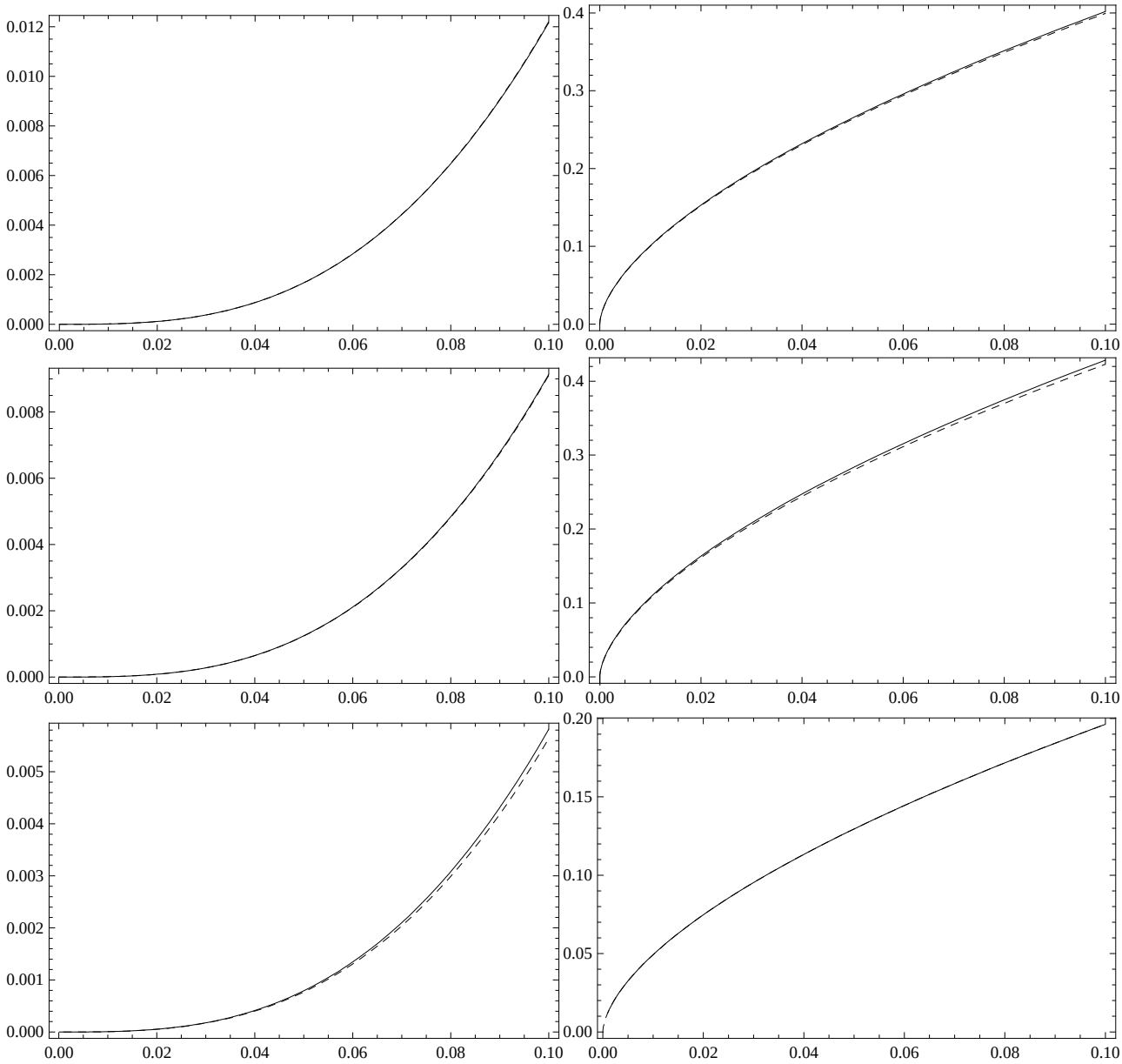

FIG. 1. Comparison of spectral fit (dashed line) and exact spectrum (solid line) for the rescaled magnetic energy density $|\rho_B(k)|^2/U$ (top panel), scalar Lorentz force $|L_B(k)|^2/U$ (middle panel) and the vector part of the anisotropic stress $|\Pi^{(V)}(k)|^2/(2U)$ (bottom panel) as a function of k/k_D with $U = (A^2 k_D^{2n_B+3})/(512\pi^4)$. In the left (right) column $n_B = 2.3$ ($n_B = -2.7$) is displayed.

Coefficients

For positive spectral indexes:

$$A_1 = -0.8998 - \frac{0.03926}{n_B} + 1.419 n_B - 0.695 n_B^2 + 0.2642 n_B^3 - 0.05418 n_B^4 + 0.004595 n_B^5$$

$$A_2 = 0.3265 + \frac{0.0008383}{n_B} + 0.01671 n_B - 0.1016 n_B^2 + 0.00989 n_B^3 - 0.002607 n_B^4 + 0.0002657 n_B^5$$

$$A_3 = 11.3 - \frac{1.631}{n_B} - 21.8 n_B + 19.66 n_B^2 - 9.243 n_B^3 + 2.184 n_B^4 - 0.2041 n_B^5$$

$$A_4 = 0.3919 + \frac{0.3111}{n_B} - 5.899 n_B + 9.607 n_B^2 - 6.21 n_B^3 + 1.79 n_B^4 - 0.1918 n_B^5$$

for the negative spectral indexes we have:

$$B_1 = \frac{1}{5}(-825 - 2848n_B - 3980n_B^2 - 2490n_B^3 - 580n_B^4) - \frac{57}{5n_B}$$
$$B_2 = \frac{1}{50}(15 - 4n_B^2)$$
$$B_3 = \frac{1}{25}(-5 - 11n_B - 8n_B^2 - 3n_B^3)$$
$$B_4 = \frac{171}{25n_B} + \frac{1}{50}(4673 + 12900n_B + 11500n_B^2 + 1950n_B^3 - 1155n_B^4)$$

for strongly negative:

$$C_1 = -\frac{10527877}{200n_B} + \frac{-126773640 - 114087370n_B - 39615180n_B^2 + 4157430n_B^3 + 7369110n_B^4 + 2081486n_B^5 + 198571n_B^6}{1000} \tag{A4}$$

2. Lorentz Force Spectra

Positive n_B

$$|L(k, n_B)|^2_{fit} = \frac{A^2 k_D^{2n_B+3}}{512\pi^4 k_*^{2n_B}}\Big(A_1^L - \frac{2}{3}\tilde{k} + A_2^L\tilde{k}^2 + A_3^L\tilde{k}^{2n_B+3}\Big) \tag{A5}$$

$-3/2 < n_B < 0$

$$|L(k, n_B)|^2_{fit} = \frac{A^2 k_D^{2n_B+3}}{512\pi^4 k_*^{2n_B}}\Big(B_1^L - \frac{2}{3}\tilde{k} + B_2^L\tilde{k}^{2n_B+3}\Big) \tag{A6}$$

$-2.9 < n_B < -3/2$

$$|L(k, n_B)|^2_{fit} = \frac{A^2 k_D^{2n_B+3}}{512\pi^4 k_*^{2n_B}}\Big(C_1^L - \frac{2}{3}\tilde{k} + C_2^L\tilde{k}^{2n_B+3}\Big) \tag{A7}$$

Coefficients

For positive spectral indexes:

$$A_1^L = 0.933635 + \frac{0.00460612}{n_B} - 0.505278n_B + 0.183487n_B^2 - 0.0238037n_B^3 - 0.00985191n_B^4 + 0.00437658n_B^5 - 0.000504247n_B^6$$
$$A_2^L = 0.22309 - \frac{0.021189}{n_B} - 0.152155n_B + 0.427087n_B^2 - 0.184484n_B^3 - 0.0111374n_B^4 + 0.0292611n_B^5 - 0.00571069n_B^6$$
$$A_3^L = 1.84015 - \frac{0.319013}{n_B} - 3.60452n_B + 2.88574n_B^2 - 0.797507n_B^3 - 0.145007n_B^4 + 0.116527n_B^5 - 0.0163659n_B^6$$

for the negative spectral indexes we have:

$$B_1^L = \frac{1}{100}(1630 + 4240n_B + 3360n_B^2 - 2080n_B^3 - 1960n_B^4 + 1970n_B^5 + 1559n_B^6) + \frac{41}{25n_B}$$
$$B_2^L = \frac{1}{100}(-854 - 2838n_B - 2710n_B^2 + 1390n_B^3 + 1705n_B^4 - 1530n_B^5 - 1340n_B^6) - \frac{4}{5n_B}$$

for strongly negative:

$$C_1^L = \frac{1}{50}(1327860 + 1077425n_B + 321980n_B^2 - 50935n_B^3 - 60380n_B^4 - 15115n_B^5 - 1302n_B^6) + \frac{60569}{5n_B}$$
$$C_2^L = -\frac{241194}{5n_B} + \frac{(-117123100 - 106256700n_B - 37275000n_B^2 + 3787200n_B^3 + 6930290n_B^4 + 1971640n_B^5 + 189111n_B^6)}{1000}$$

3. Vector Spectra

Positive n_B

$$|\Pi^{(V)}(k,n_B)|^2_{fit} = \frac{A^2 k_D^{2n_B+3}}{256\pi^4 k_*^{2n_B}}\Big(A_1^V - \frac{5}{12}\tilde{k} + A_2^V + A_3^V \tilde{k}^{2n_B+3}\Big) \tag{A8}$$

$-3/2 < n_B < 0$

$$|\Pi^{(V)}(k,n_B)|^2_{fit} = \frac{A^2 k_D^{2n_B+3}}{256\pi^4 k_*^{2n_B}}\Big(B_1^V - \frac{5}{12}\tilde{k} + B_2^V \tilde{k}^2 + B_3^V \tilde{k}^{2n_B+3}\Big) \tag{A9}$$

$-2.9 < n_B < -3/2$

$$|\Pi^{(V)}(k,n_B)|^2_{fit} = \frac{A^2 k_D^{2n_B+3}}{256\pi^4 k_*^{2n_B}}\Big(C_1^V - \frac{5}{12}\tilde{k} + C_2^V \tilde{k}^{2n_B+3}\Big) \tag{A10}$$

Coefficients
For positive spectral indexes:

$$A_1^V = \frac{29500 - 16100 n_B + 5850 n_B^2 - 765 n_B^3 - 314 n_B^4 + 140 n_B^5 - 16 n_B^6}{50000}$$
$$A_2^V = \frac{-845 + 2600 n_B - 690 n_B^2 + 124 n_B^3}{10000}$$
$$A_3^V = \frac{1}{500}(-280 + 545 n_B - 425 n_B^2 + 112 n_B^3)$$

for the negative spectral indexes we have:

$$B_1^V = \frac{26}{25 n_B} + \frac{1}{100}(1040 + 2698 n_B + 2140 n_B^2 - 1327 n_B^3 - 1249 n_B^4 + 1255 n_B^5 + 992 n_B^6)$$
$$B_2^V = \frac{1}{100}(-2192 - 4681 n_B - 2132 n_B^2 + 2235 n_B^3 + 908 n_B^4 - 1464 n_B^5 - 744 n_B^6) - \frac{53}{20 n_B}$$
$$B_3^V = \frac{73}{50 n_B} + \frac{1}{100}(1078 + 1616 n_B - 243 n_B^2 - 735 n_B^3 + 471 n_B^4 + 59 n_B^5 - 342 n_B^6)$$

for strongly negative:

$$C_1^V = \frac{445985}{500 n_B} + \frac{(19923100 + 16525360 n_B + 5113265 n_B^2 - 742742 n_B^3 - 956890 n_B^4 - 246837 n_B^5 - 21843 n_B^6}{1000}$$
$$C_2^V = \frac{-29003653 - 25196700 n_B - 8371900 n_B^2 + 995460 n_B^3 + 1561850 n_B^4 + 429404 n_B^5 + 40254 n_B^6}{1000} - \frac{124807}{10 n_B}$$

Appendix B: Cross Correlators Exact Solutions

To give the reader an idea of the complete analytical form of the Lorentz force and energy density cross correlator we show the exact results for two representative spectral indices $n_B = 2$ and $n_B = -2.5$:

$$\langle \rho_B(k) L_B(k)\rangle|_{n_B=2} = \frac{A^2 k_D^7}{1024\pi^5 a^8}\Big[-\frac{4}{21} + \frac{\tilde{k}}{2} - \frac{8\tilde{k}^2}{15} + \frac{\tilde{k}^3}{6} + \frac{\tilde{k}^5}{96} - \frac{3\tilde{k}^7}{1120}\Big]$$
$$\langle \rho_B(k) L_B(k)\rangle|_{n_B=-5/2} = \frac{A^2}{1024\pi^5 a^8 k_D^2}\Big[\frac{16(4 - 65\tilde{k} + 59\tilde{k}^2 - 2\tilde{k}^3 + 4\tilde{k}^4)}{(105\sqrt{|1-\tilde{k}|}\tilde{k}^3)} - \frac{64 + 448\tilde{k}^2 + 42\tilde{k}^4}{105\tilde{k}^3}\Big] \tag{B1}$$

where $\tilde{k} = k/k_D$. In Fig. 2 we show the comparison between the energy density the Lorentz force and their cross correlation for $n_B = -2.5$ and $n_B = 2$: the cross-correlation is negative in the whole range of scales. In Fig. 3 we show the impact of various assumptions for the cross-correlation between the magnetic energy density and the Lorentz force on the power spectrum of CMB temperature anisotropies.

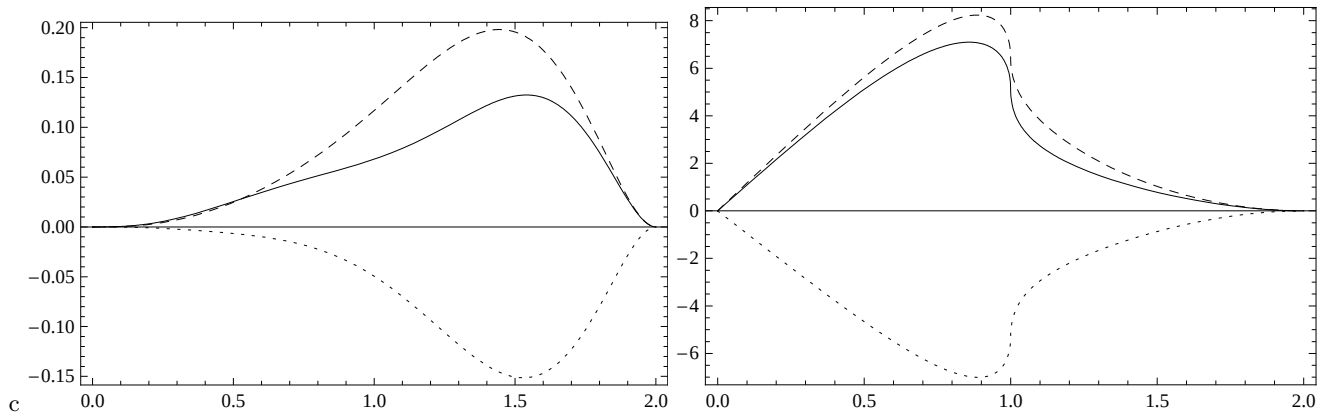

FIG. 2. The cross-correlator $k^3\langle\rho_B(k)L_B(k)\rangle/U$ (dotted line) for $n_B = 2$ and $n_B = -5/2$ is plotted versus k/k_D in comparison with $k^3|\rho_B(k)|^2/U$ (solid line) and $k^3|L_B(k)|^2/U$ (dashed line) with $U = (A^2 k_D^{2n_B+3})/(512\pi^4)$.

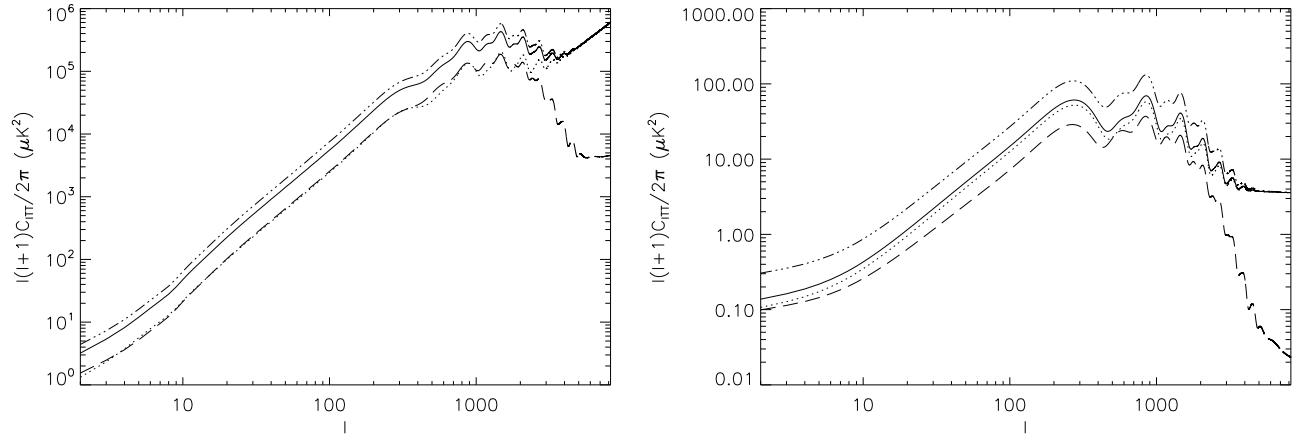

FIG. 3. We computed the scalar power spectrum with the contribution of the Lorentz force-energy density cross correlation for $n_B = 2$ (top panel) and $n_B = -2.5$ (bottom panel). Solid line represents the correct assumption on the cross-correlation, the dotted line represents the result considering the Lorentz force and the energy density fully anti-correlated, triple dotted-dashed line represents the uncorrelated sum and the dashed line represents the result assuming full correlation.

Appendix C: Scalar Initial Conditions with Matter Corrections

We computed the initial conditions for magnetized scalar perturbations for the leading regular growing mode which is the one which contributes to CMB anisotropies, we do not consider any isocurvature or decaying modes. Initial conditions are the solution of the coupled Einstein Boltzmann equation system with PMF contributions on long wavelenghts at early epochs. The Einstein equations with the contribution of PMF in the synchronous gauge (with the notation of [36]) are:

$$
\begin{aligned}
&k^2\eta - \frac{1}{2}\mathcal{H}\dot{h} = -4\pi G a^2(\Sigma_n\,\rho_n\delta_n + \rho_B)\,,\\
&k^2\dot{\eta} = 4\pi G a^2\Sigma_n(\rho_n + P_n)\theta_n\,,\\
&\ddot{h} + 2\mathcal{H}\dot{h} - 2k^2\eta = -8\pi G a^2\Big(\Sigma_n\, c_{s\,n}^2\rho_n\delta_n + \frac{\delta\rho_B}{3}\Big)\,,\\
&\ddot{h} + 6\ddot{\eta} + 2\mathcal{H}(\dot{h} + 6\dot{\eta}) - 2k^2\eta = -24\pi G a^2[\Sigma_n(\rho_n + P_n)\sigma_n + \sigma_B],
\end{aligned}
\tag{C1}
$$

where n represents the various species of the plasma: b for baryons, c for cold dark matter (CDM), γ for photons and ν for massless neutrinos. The scalar metric perturbations are represented by the two scalar potential h, η while fluid perturbations are represented by δ_i, θ_i, σ_i which are respectively the density contrast the fluid velocity and the

anisotropic stress in the notation of [36]. The overdots denote the derivative with respect to conformal time. On long wavelenght we can expand the metric and fluid perturbations in series of $k\tau << 1$. In our previous works [8, 9] we computed the intial conditions deep in the radiation era with the approximation of a universe dominated only by relativistic degrees of freedom (radiation and massless neutrinos). Usually considering $a(\tau) \propto \tau$ is a rather good approximation for setting the initial conditions (see however Ref. [30] for a different claim stressing the importance of matter corrections). We have therefore extended our previous results [9] to the case in which the matter contribution is taken into account. Considering the matter contribution in the initial condition needs the introduction of matter correction also in the evolution of the scale factor [45]:

$$a(\tau) = \frac{\Omega_m H_0^2}{\omega^2}\Big(\omega\tau + \frac{1}{4}\omega^2\tau^2\Big)\,,$$
$$\omega = \frac{\Omega_m H_0}{\sqrt{\Omega_\nu + \Omega_\gamma}}\,,$$

where $\Omega_m = \Omega_c + \Omega_b$ and the Hubble parameter can be expanded as $\mathcal{H} \propto \frac{1}{\tau} + \frac{\omega}{4}$. The Einstein equations become:

$$k^2\eta - \frac{1}{2}\mathcal{H}\dot{h} = -4\pi G a^2(\rho_\gamma\delta_\gamma + \rho_\nu\delta_\nu + \rho_b\delta_b + \rho_c\delta_c + (\rho_\nu + \rho_\gamma)\Omega_B)\,, \tag{C2}$$

$$k^2\dot{\eta} = 4\pi G a^2\left(\frac{4}{3}\rho_\gamma\theta_\gamma + \frac{4}{3}\rho_\nu\theta_\nu + \rho_b\theta_b\right)\,, \tag{C3}$$

$$\ddot{h} + 2\mathcal{H}\dot{h} - 2k^2\eta = -8\pi G a^2\left[\frac{1}{3}\rho_\gamma\delta_\gamma + \frac{1}{3}\rho_\nu\delta_\nu + \frac{1}{3}(\rho_\gamma + \rho_\nu)\Omega_B\right]\,, \tag{C4}$$

$$\ddot{h} + 6\ddot{\eta} + 2\mathcal{H}(\dot{h} + 6\dot{\eta}) - 2k^2\eta = -24\pi G a^2\left[\frac{4}{3}\rho_\nu\delta_\nu + (\rho_\nu + \rho_\gamma)\Big(\frac{\Omega_B}{3} + L_B\Big)\right]\,, \tag{C5}$$

where PMF contributions are given in terms of their ratio with the fluid radiation density: $\Omega_B = \rho_B/\rho_{rad}$, $L_B = L_B/\rho_{rad}$ and $\sigma_B = \sigma_B/\rho_{rad}$ (with $\rho_{rad} = \rho_\nu + \rho_\gamma$). The initial conditions at leading order with PMFs which include the matter corrections are:

$$\begin{aligned}
h(k,\tau) &= -\frac{3}{4}\Omega_B\omega\tau + \frac{9}{32}\Omega_B\omega^2\tau^2\\
\eta(k,\tau) &= \frac{1}{8}\Omega_B\omega\tau - \frac{3\Omega_B\omega^2\tau^2}{64} + \frac{(-165L_B - 55\Omega_B + 28R_\nu\Omega_B)}{168(15+4R_\nu)}k^2\tau^2\\
\delta_\gamma(k,\tau) &= -\Omega_B + \frac{\Omega_B\omega\tau}{2} - \frac{3\Omega_B\omega^2\tau^2}{16} - \frac{(3L_B + \Omega_B - R_\nu\Omega_B)}{6(-1+R_\nu)}k^2\tau^2\\
\delta_\nu(k,\tau) &= -\Omega_B + \frac{\Omega_B\omega\tau}{2} - \frac{3\Omega_B\omega^2\tau^2}{16} - \frac{(3L_B + \Omega_B - R_\nu\Omega_B)}{6R_\nu}k^2\tau^2\\
\delta_b(k,\tau) &= -3\frac{\Omega_B}{4} + \frac{3\Omega_B\omega\tau}{8} + \frac{1}{8}k^2\tau^2\Omega_B - \frac{9}{64}\Omega_B\omega^2\tau^2\omega^2 - \frac{3L_Bk^2\tau^2}{8(-1+R_\nu)}\\
\delta_c(k,\tau) &= -\frac{3\Omega_B}{4} + \frac{3\Omega_B\omega\tau}{8} - \frac{9}{64}\Omega_B\omega^2\tau^2\\
\theta_\gamma(k,\tau) &= \frac{3L_Bk^2\tau}{4(-1+R_\nu)} - \frac{\Omega_B}{4}k^2\tau + k^2\tau^2\left[-\frac{9L_B(-1+R_c)\omega}{16(-1+R_\nu)^2} + \frac{(-4+R_\nu+3R_c)\omega\Omega_B}{16(-1+R_\nu)}\right]\\
\theta_\nu(k,\tau) &= \frac{3L_Bk^2\tau}{4R_\nu}) - \frac{k^2(-1+R_\nu)\Omega_B\tau}{4R_\nu} + \frac{1}{16}k^2\tau^2\omega\Omega_B\\
\theta_b(k,\tau) &= \frac{3L_Bk^2\tau}{4(-1+R_\nu)} - \frac{1}{4}\Omega_Bk^2\tau + k^2\tau^2\left[-\frac{9L_B(-1+R_c)\omega}{16(-1+R_\nu)^2} + \frac{(-4+R_\nu+3R_c)\omega\Omega}{16(-1+R_\nu)}\right]\\
\theta_c(k,\tau) &= 0\\
\sigma_\nu(k,\tau) &= -\frac{3L_B+\Omega_B}{4R_\nu} + \frac{\Omega_Bk^2(55-28R_\nu)\tau^2}{56R_\nu(15+4R_\nu)} + \frac{165L_Bk^2\tau^2}{56R_\nu(15+4R_\nu)}\\
F_3(k,\tau) &= -\frac{3k\tau(3L_B+\Omega_B)}{14R_\nu} + \frac{165L_B+55\Omega_B-28R_\nu\Omega_B}{7(430R_\nu+112R_\nu^2)}\,,
\end{aligned} \tag{C6}$$

where $R_\nu = \rho_\nu/(\rho_\nu + \rho_\gamma)$. We note that our results are in agreement, within our notation, with the one presented in [10]. We verified that the inclusion of the matter correction in the initial conditions in our modified `CAMB` code does

not produce any appreaciable change in the results: $\Delta C_l/C_l \sim 10^{-5}$ which is the level of numerical noise, in contrast with Ref. [30].

[1] L. M. Widrow, Rev. Mod. Phys. **74** (2002) 775
[2] M. L. Bernet, F. Miniati, S. J. Lilly, P. P. Kronberg and M. Dessauges-Zavadsky, Nature **454** (2008) 302
[3] A. M. Wolfe, R. A. Jorgenson, T. Robishaw, C. Heiles and J. X. Prochaska, Nature **455** (2008) 638
[4] S. Koh and C. H. Lee, Phys. Rev. D **62**, 083509 (2000).
[5] D. G. Yamazaki, K. Ichiki, T. Kajino and G. J. Mathews, Ap. J. 646, 719 (2006).
[6] T. Kahniashvili and B. Ratra, Phys. Rev. D 75, 023002 (2007).
[7] M. Giovannini and K. Kunze, Phys. Rev. D 77, 063003 (2008).
[8] F. Finelli, F. Paci and D. Paoletti, Phys.Rev. D **78**, 023510 (2008).
[9] D. Paoletti, F. Finelli and F. Paci, MNRAS 396, 523 (2009).
[10] J. R. Shaw and A. Lewis, Phys. Rev. **D 81**, 043517 (2010).
[11] C. Bonvin and C. Caprini, JCAP 1005:022 (2010).
[12] K. Subramanian and J. D. Barrow, Phys. Rev. D 58, 083502 (1998).
[13] A. Mack, T. Kahniashvili and A. Kosowsky, Phys. Rev. D 65, 123004 (2002).
[14] A. Lewis, Phys. Rev. D, 70, 043011 (2004).
[15] R. Durrer, P. G. Ferreira and T. Kahniashvili, Phys. Rev. D 61, 043001 (2000).
[16] C. Caprini, R. Durrer and T. Kahniashvili, Phys. Rev. D 69, 063006 (2004).
[17] I. Brown and R. Crittenden, Phys. Rev. D 72, 063002 (2005).
[18] T. R. Seshadri and K. Subramanian, Phys. Rev. Lett. 103, 081303 (2009).
[19] C. Caprini, F. Finelli, D. Paoletti and A. Riotto, JCAP 0906:021 (2009).
[20] A. Lewis and S. Bridle, Phys. Rev. D 66, 103511 (2002).
[21] A. Lewis, A. Challinor and A. Lasenby, Astrophys. J. 538, 473 (2000).
[22] D. G. Yamazaki, K. Ichiki, T. Kajino and G. J. Mathews, Phys. Rev. D **81** (2010) 023008
[23] J. R. Shaw and A. Lewis, arXiv:1006.4242 [astro-ph.CO].
[24] [Planck Collaboration] "Planck: The scientific programme," (2006), ArXiv: 0604.069 [astro-ph].
[25] N. Jarosik *et al.*, Astrophys. J. S. **192** (2011) 14.
[26] D. Larson *et al.*, Astrophys. J. S. **192** (2011) 16.
[27] C. L. Reichard et al., Astrophys. J. 694, 1200-1219 (2009).
[28] H. C. Chiang et al., 2009, "Measurements of CMB Polarization Spectra From Two Years BICEP Data," ArXiv:0906.1181 [astro-ph].
[29] M. L. Brown *et al.* [QUaD collaboration], Astrophys. J. **705** 978 (2009)
[30] K. Kojima and K. Ichiki, arXiv:0902.1367 [astro-ph] (2009).
[31] F. Finelli, J. Hamann, S. M. Leach and J. Lesgourgues, JCAP **1004** (2010) 011.
[32] S. Seager, D. D. Sasselov, and D. Scott, Astrophys. J. **523** (1999) L1.
[33] J. L. Sievers *et al.*, Astrophys. J. **660** (2007) 976
[34] M. Tegmark et al., Phys. Rev. D 74, 123507, (2006)
[35] S. Cole et al. (The 2dFGRS), Mon. Not. Roy. Astron. Soc. **362**, 505 (2005)
[36] C. P. Ma and E. Bertschinger, Astrophys. J. 455, 7 (1995).
[37] E. Komatsu and U. Seljak, MNRAS **336**, 1256 (2002).
[38] W. K. Hastings, Biometrika 57(1), 97 (1970).
[39] A. Gelman and D. B. Rubin, Statistical Science 7, 457 (1992)
[40] N. Mandolesi et al., A & A **520** (2010) A3.
[41] J.-M. Lamarre et al., A & A **520** (2010) A9.
[42] R. Durrer and C. Caprini, JCAP **0311** (2003) 010
[43] We thank Ruth Durrer for raising the issue of a logarithmic prior for B_lambda.
[44] W. Valkenburg, J. Hamann and L. M. Krauss, Phys. Rev. D **78** (2008) 063521
[45] A. Lewis, "CAMB Notes", available at http://cosmologist.info.

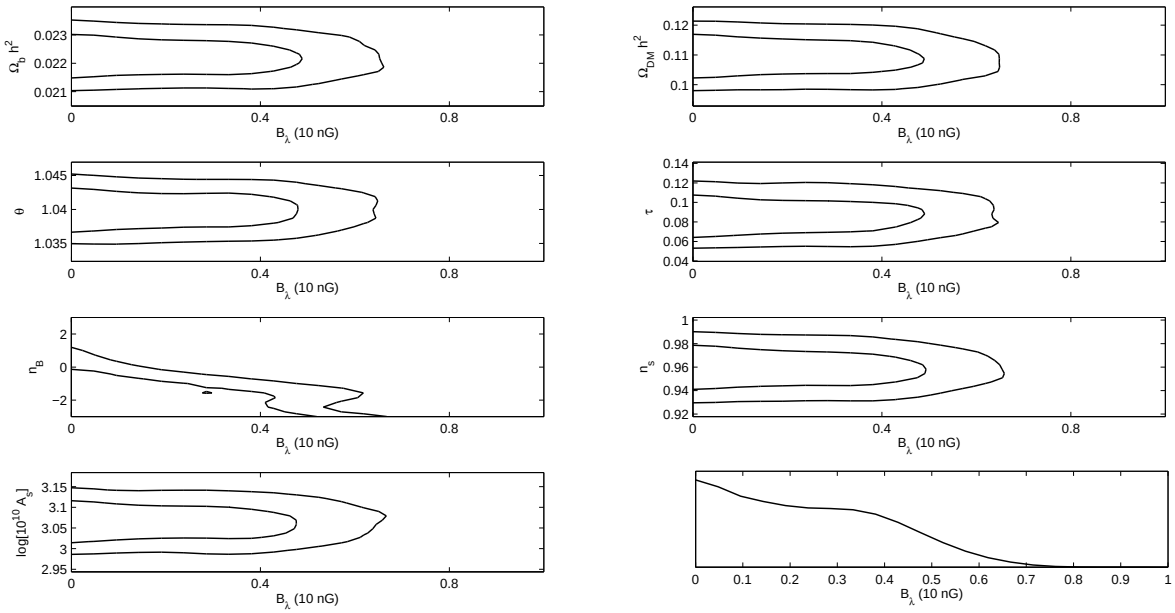

FIG. 4. Results of the MCMC constrained with WMAP 7 years, BICEP, QUaD and ACBAR data. Curves are the 68% and 95% confidence level. Note that B_λ (with $\lambda = 1$ Mpc) is in 10 nG units.

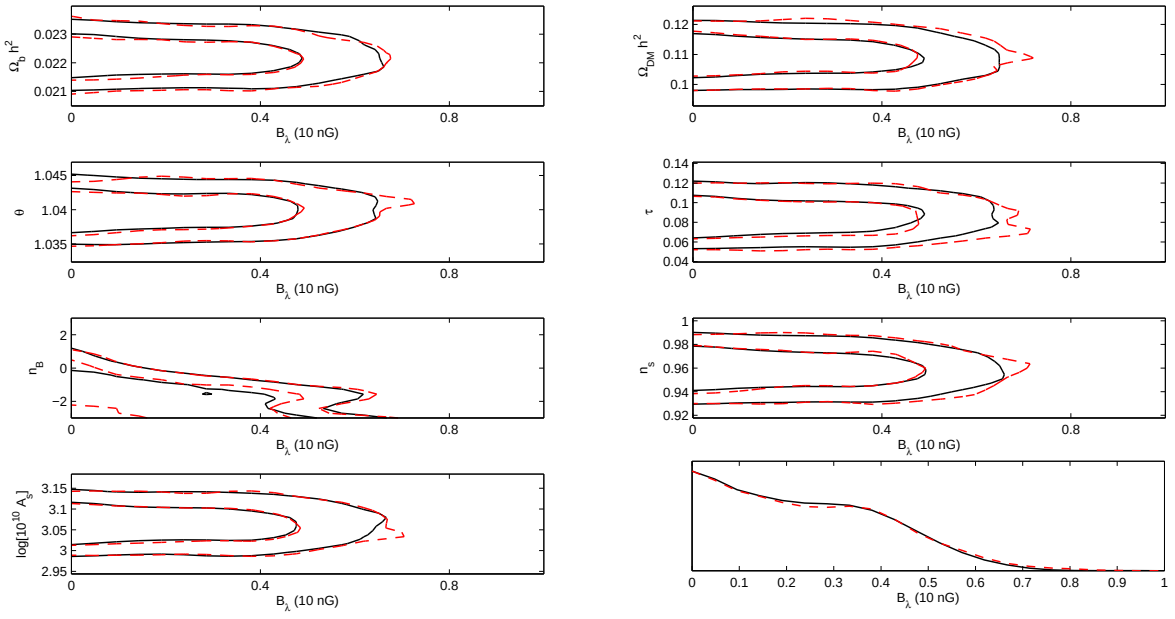

FIG. 5. Results of the MCMC constrained with WMAP 7 years, BICEP, QUaD and ACBAR data. Curves are the 68% and 95% confidence level. Solid lines are the results considering both scalar and vector magnetic modes while dashed lines are the results taking into account only the vector contribution. Note that B_λ (with $\lambda = 1$ Mpc) is in 10 nG units.

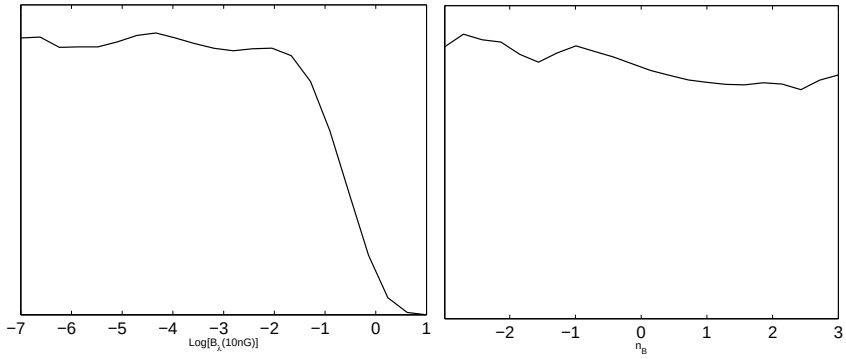

FIG. 6. Results of the MCMC for the PMF spectral index constrained with WMAP 7 years, BICEP, QUaD and ACBAR data and logarithmic prior for the PMF amplitude. Curves are the 95% and 68% confidence level.

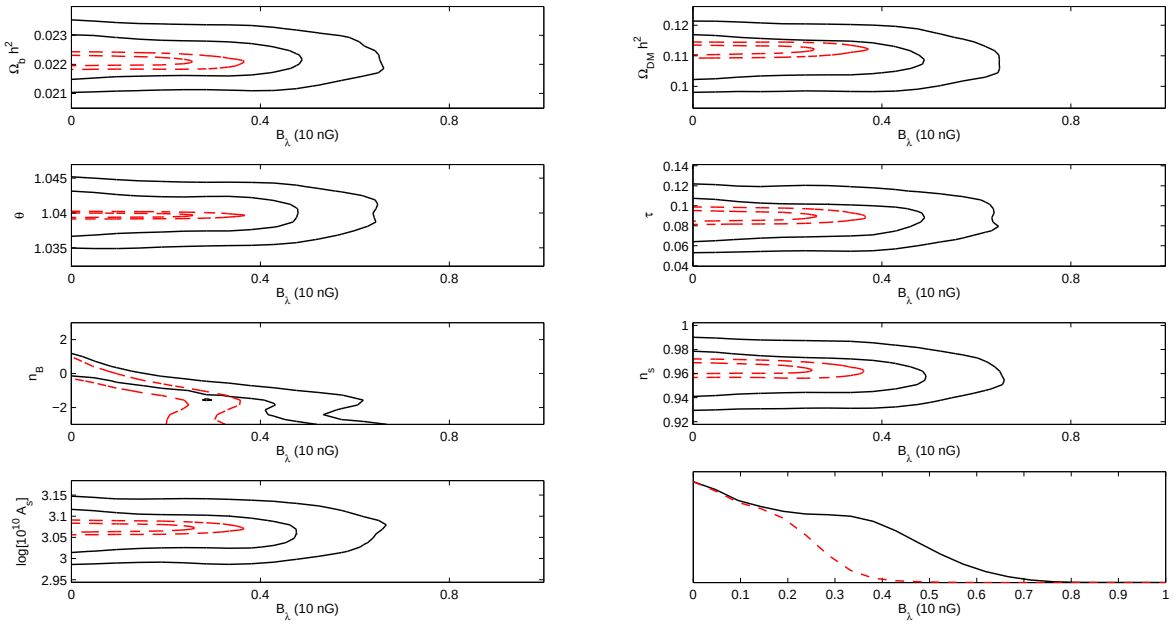

FIG. 7. Comparison of the results of the MCMC with real data used in Figs. 5, 6 (solid line) and simulated Planck data (dashed line). Curves are the 95% and 68% confidence level. Note that B_λ (with $\lambda = 1$ Mpc) is in 10 nG units. Note that k_D is a derived parameter.